Aalto University

Aaltodoc
OPEN ACCESS

This is an electronic reprint of the original article.
This reprint may differ from the original in pagination and typographic detail.

Author(s): Manderbacka, Teemu & Mikkola, Tommi & Ruponen, Pekka & Matusiak, Jerzy

Title: Transient response of a ship to an abrupt flooding accounting for the momentum flux

Year: 2015

Version: Post print

Please cite the original version:

Manderbacka, Teemu & Mikkola, Tommi & Ruponen, Pekka & Matusiak, Jerzy. 2015. Transient response of a ship to an abrupt flooding accounting for the momentum flux. Journal of Fluids and Structures. Volume 57. 108-126. ISSN 0889-9746 (printed). DOI: 10.1016/j.jfluidstructs.2015.06.001.

Rights: © 2015 Elsevier BV. This is the post print version of the following article: Teemu Manderbacka, Tommi Mikkola, Pekka Ruponen, Jerzy Matusiak, Transient response of a ship to an abrupt flooding accounting for the momentum flux, Journal of Fluids and Structures, Volume 57, August 2015, Pages 108-126, ISSN 0889-9746, http://dx.doi.org/10.1016/j.jfluidstructs.2015.06.001, which has been published in final form at http://www.sciencedirect.com/science/article/pii/S0889974615001310

All material supplied via Aaltodoc is protected by copyright and other intellectual property rights, and duplication or sale of all or part of any of the repository collections is not permitted, except that material may be duplicated by you for your research use or educational purposes in electronic or print form. You must obtain permission for any other use. Electronic or print copies may not be offered, whether for sale or otherwise to anyone who is not an authorised user.

*Manuscript
Click here to view linked References

Transient response of a ship to an abrupt flooding accounting for the momentum flux

T. Manderbacka[a,*], T. Mikkola[a], P. Ruponen[b], J.E. Matusiak[a]

[a] *Aalto University, School of Engineering, Department of Applied Mechanics, Helsinki, Finland*
[b] *Napa Ltd, Helsinki, Finland*

Abstract

Numerical non-linear time domain simulation method for damaged ship motions is presented. Floodwater motion modelling is based on the lumped mass method with a moving free surface. The ship and floodwater motions are fully coupled. The variation of the floodwater mass is accounted for. A model to account for the flooding ingress transporting the momentum is presented. The experiments of abrupt flooding have shown that the ship may experience the first large roll towards the undamaged side, especially when a large undivided compartment is flooded. The presented time domain model is validated against the experimental data on the roll damping of the flooded ship and transient flooding. Two different initial stability conditions and two different compartment layouts are studied. Viscous dissipation of the floodwater motions is modelled with an equivalent friction coefficient. The impact of the viscous damping is studied. Transient flooding tests show that the inflow momentum has to be accounted for when the undivided compartment is flooded. The simulation model is capable of capturing the impact of the inflooding jet and the first roll on the opposite side of the damage is reproduced.

Keywords: time domain simulation, floodwater progression, floodwater motion, lumped mass, sloshing, damage stability

*Corresponding author
Email address: teemu.manderbacka@aalto.fi (T. Manderbacka)

1. Introduction

The loss of hull integrity of a ship leading to flooding can be a severe risk to the ship stability. The flooding process can be divided into three stages; I) transient stage, where the water starts to ingress the ship, II) progressive stage, where the flooding is more quasi-static and III) steady state, where final equilibrium angle is reached but the ship may experience roll motions due to wave excitation (Ruponen, 2007). This study concentrates on the flooding process at the transient stage. The roll response is of particular interest, since it is the most sensitive motion component with regards to the flooding. Collision or grounding can cause a large opening on the ship hull. In this case the flooding can be fast at the beginning. If the damage extent is not large enough, to cause immediate foundering or total loss of stability, the dynamic roll angles may still be dangerously large at the transient stage leading to capsize.

An abrupt asymmetric flooding, when the obstructions in the flooded compartment slow down the cross-flooding, may cause a large roll on the damage side and even a capsize (Spouge, 1985). The asymmetric flooding has been studied experimentally and numerically by Vredeveldt and Journée (1991); Journée et al. (1997); Santos et al. (2002). In the experiments on

the transient flooding of large open spaces (Ikeda and Ma, 2000; de Kat and van't Veer, 2001; Ikeda and Kamo, 2001; Ikeda et al., 2003; Manderbacka et al., 20xx) it has been observed that the ship may also roll first on the opposite side of the damage. The inflooding jet can push the floodwater to the opposite side and cause the first large roll on that side. In this case the flooding may be slowed down or even stopped when the opening is lifted due to the roll on the opposite side. This may lead to a different final equilibrium position. Previous studies point out the fact that the intermediate stages of flooding can vary significantly from the final equilibrium stage depending on the flooding process. This process can be complex (Khaddaj-Mallat et al., 2011), including the inflooding jet, sloshing and viscous effects. These, in turn, are all affected by the ship motions. The ship response and the flooding process are coupled. Inflow jet transports inflooding water with momentum into the damaged ship (ITTC, 2014). The viscous effects and wave breaking may dampen the sloshing (Bouscasse et al., 2014a,b) and affect on the progression of the flooding during the intermediate stages. Furthermore, the trapped air may slow down the flooding process (Palazzi and de Kat, 2004; Ruponen et al., 2013). In addition to the above mentioned

In order to assess the consequences of a flooding accident, water ingress and ship motions need to be simulated in time domain. Flooding simulation tools of increasing complexity can be divided into four main groups. (1) Quasi-static methods assume horizontal water surface in flooded compartments. They are mainly aimed to simulate the progressive stage of the flooding (de Kat, 2000; van't Veer and de Kat, 2000; Santos et al., 2002; Ruponen et al., 2007; Santos and Guedes Soares, 2009; Ypma and Turner,

2010; Schreuder et al., 2011; Dankowski, 2012). These numerical methods have been applied to simulate transient flooding in the asymmetric flooding cases. The roll response to the asymmetric flooding has been captured by these codes when the floodwater motions are limited due to the obstructions in the compartments. (2) Lumped mass models with a moving plane free surface (Papanikolaou et al., 2000; Spanos and Papanikolaou, 2001; Jasionowski, 2001; Fujiwara and Haraguchi, 2005; Valanto, 2008) account for the dynamic effect of the floodwater motions by a moving point mass concentrated at the center of gravity of floodwater as presented by Zaraphonitis et al. (1997). (3) Shallow water equation models (Dillingham, 1981; Chang and Blume, 1998; Santos and Guedes Soares, 2008; Valanto, 2008) for sloshing apply a random choice method (Glimm's method) to solve the shallow water equations in a numerical grid in the flooded compartment. Chang and Blume (1998) apply the method for floodwater depths smaller than 15 % of the compartment width, while Valanto (2008) sets the limit to 25 %.

Lumped mass models with moving free surface (2) and shallow water equation models (3) have been mainly applied to simulate the damage ship response in waves. In these cases the transient flooding stage has not been covered. The transient stage of flooding has been simulated by (4) Computional Fluid Dynamics (CFD) codes only for very specific problems. Naito and Sueyoshi (2001) show the applicability of the Smoothed Particle Hydrodynamics (SPH) method to simulate the sloshing on deck in forced ship motions. Shen and Vassalos (2009) apply Volume of Fluid (VOF) and SPH simulations for a 2D box case. Gao et al. (2011) simulate the progressive flooding of the ITTC benchmark barge (Ruponen et al., 2007). They show

the applicability of the VOF method to simulate the free floating ship motions. However, in this case the measured roll angles were less than 0.25 deg. Several flooding cases are simulated with CFD by Sadat-Hosseini et al. (2012) applying single-phase level set approach. In their study there were some differences with roll motion in the flooding simulation but the free surface shape was well captured. Three dimensional SPH simulation has been applied by Touzé et al. (2010) for a stationary compartment abrupt flooding. Hashimoto et al. (2013) simulate the abrupt flooding with moving particle semi-implicit method (MPS) coupled with potential flow model. Souto-Iglesias et al. (2013, 2014) discuss the consistency of the MPS method and the equivalence between the SPH and MPS methods.

Number of studies cover the damage ship motions in waves. However, there is very little information on the transient flooding. In the benchmark studies of the 23rd and 24th ITTC (2002, 2005) it was noted that the detailed modelling of the coupled ship and floodwater motions should be studied more carefully. Benchmark study by the 24th ITTC (2005) compared the performance of five different codes to predict the dynamic motions of damaged ship. Participating codes included; (1) quasi-static, (2) lumped mass with a moving free surface and (3) shallow water equation methods. The lumped mass with a moving free surface methods were noted to have the best agreement with the experimental data. Later, ITTC (2008, 2011) report several improvements in the codes simulating progressive flooding and damaged ship in waves. The 27th ITTC (2014) points out the importance of correct modelling of the floodwater effects on damping of roll and the inertia of floodwater entering the ship. The first three of the above mentioned categories of tools

apply the Bernoulli equation based hydraulic model to calculate the flooding rate through the openings. In CFD application no separate model for the flow through the opening is required. CFD methods are often proposed to solve the complicated coupled problems. Still, the required calculation times are long. The modelling of compartment spaces is cumbersome, even more so in case of complicated compartment spaces, like the ones of the cruise vessels.

An effective method is needed in practice for the purpose of marine traffic safety analysis. It is important to study in which conditions the simplified methods can be applied and is it possible to extend their limits with adequate submodels. This work aims to validate the applicability of the lumped mass with moving free surface method to predict the transient response on the abrupt flooding. It concentrates on the ship motions coupled with; the inflooding jet, floodwater motions and the flow through the openings. A model accounting for the mass variation in the compartment and the in/egress momentum flux is presented. This allows for the simulation of the inflooding jet. The transient flooding cases where the inflooding jet plays an important role have not been simulated before to the authors knowledge.

Damaged ship motions are simulated for the system consisting of the ship considered as a rigid body with constant inertia properties and of the lumped masses representing the water at each flooded space in the ship. Degrees of freedom for the system are dependent on the number of flooded spaces in the ship. First the equations of motion for an intact ship are presented in section 2 and then the equations for the lumped masses in section 3 and finally the combination of these into one system is presented in section 4.

The mass in each compartment is changing due to the progression of flooding through the openings. This is modelled with hydraulic equation assuming quasi-stationary flow at the opening. The ship and lumped mass motions i.e. sloshing are taken into account in the model for flow through the opening. Model is validated against the model test data of the transient flooding in calm water, where the flooded compartments were fully ventilated. This way the uncertainties of the wave action and the air compression were evaded. The validation cases are presented in section 5. The results of the simulations are compared with the measurement data in section 6 and they are discussed in section 7. The main conclusions are pointed out in section 8.

2. Model for the ship motions

Two coordinate systems shown in Figure 1 are applied, the inertial coordinate frame **XYZ** and the body fixed coordinate frame **xyz** fixed to the intact ship center of gravity *cog*. Ship position is expressed in the inertial coordinate frame with vector $\mathbf{R} = \{X, Y, Z\}^T$ and the angular attitude with $\mathbf{\Theta} = \{\phi, \theta, \psi\}^T$. The angular attitude is expressed with modified Euler angles where the order of rotations is; yaw ψ (around **z**-axis), pitch θ (around **y**-axis) and roll ϕ (around **x**-axis).

2.1. Equations of motion for the intact ship

General equations of motion for a rigid body are written in the ship coordinate system **xyz**. These equations in the vector form are (Fossen,

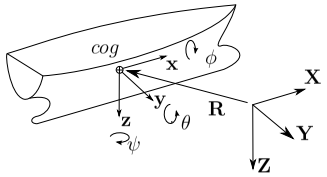

Figure 1: Coordinate systems.

2002)

$$m\left[\dot{\mathbf{U}} + \mathbf{\Omega} \times \mathbf{U}\right] = \mathbf{f}_{tot} \quad (1)$$

$$\mathbf{I}_S\dot{\mathbf{\Omega}} + \mathbf{\Omega} \times \mathbf{I}_S\mathbf{\Omega} = \boldsymbol{\tau}_{tot}\ , \quad (2)$$

where m is the ship mass, $\mathbf{U} = \{u, v, w\}^T$ is the velocity of the ship, $\mathbf{\Omega} = \{p, q, r\}^T$ is the angular velocity of the ship, $\mathbf{I}_S$ is the ship rotational inertia matrix, $\mathbf{f}_{tot}$ is a vector including all the external forces acting on the ship and the $\boldsymbol{\tau}_{tot}$ is a moment vector of all the external moments acting on the ship center of gravity.

The above Equations 1 and 2 can be written in a matrix form as

$$\mathbf{M}_S \begin{Bmatrix} \dot{\mathbf{U}} \\ \dot{\mathbf{\Omega}} \end{Bmatrix} + \mathbf{C}_S(\mathbf{U}, \mathbf{\Omega}) \begin{Bmatrix} \mathbf{U} \\ \mathbf{\Omega} \end{Bmatrix} = \begin{Bmatrix} \mathbf{f}_{tot} \\ \boldsymbol{\tau}_{tot} \end{Bmatrix}\ , \quad (3)$$

where $\mathbf{M}_S$ and $\mathbf{C}_S(\mathbf{U}, \mathbf{\Omega})$ are the ship mass- and centripetal-mass matrices

$$\mathbf{M}_S = \begin{bmatrix} m\mathbf{I}_{3\times3} & \mathbf{0}_{3\times3} \\ \mathbf{0}_{3\times3} & \mathbf{I}_S \end{bmatrix} \quad (4)$$

and

$$\mathbf{C}_S(\mathbf{U}, \mathbf{\Omega}) = \begin{bmatrix} \mathbf{0}_{3\times3} & -S(m\mathbf{U}) \\ \mathbf{0}_{3\times3} & -S(\mathbf{I}_S\mathbf{\Omega}) \end{bmatrix}\ , \quad (5)$$

where the $\mathbf{I}_{3\times3}$ and $\mathbf{0}_{3\times3}$ are identity and zero matrices of size 3×3. The cross product is performed by multiplication with matrix $\mathbf{S}(\cdot)$, as $\mathbf{a} \times \mathbf{b} = \mathbf{S}(\mathbf{a})\ \mathbf{b}$, where

$$\mathbf{S}(\mathbf{a}) = \begin{bmatrix} 0 & -a_z & a_y \\ a_z & 0 & -a_x \\ -a_y & a_x & 0 \end{bmatrix} . \tag{6}$$

2.2. External forces acting on the ship

The total external force vector consists of the gravity, hydrostatic and radiation forces. Wave action is not accounted for. The gravitation force vector acting on the ship expressed in the ship fixed coordinate system as a function of the ship angular position $\mathbf{\Theta} = \{\phi, \theta, \psi\}$ is $\mathbf{f}_g(\mathbf{\Theta}) = m\mathbf{g}(\mathbf{\Theta})$, where the gravitation vector $\mathbf{g}(\mathbf{\Theta})$ is expressed in the ship coordinate system. Ship coordinate system is located at the ship *cog* thus the gravity does not cause any moment to the ship.

The hydrostatic forces $\{\mathbf{f}_H(\mathbf{R}, \mathbf{\Theta}), \boldsymbol{\tau}_H(\mathbf{R}, \mathbf{\Theta})\}^T$ acting on the ship hull are integrated from the hydrostatic pressure over the actual wetted surface of the hull at ship position $\mathbf{R}$,$\mathbf{\Theta}$. The hull is presented with triangular panels. Panel area, normal and center point position are applied to calculate the hydrostatic forces. Pressure is calculated at the panel center point. Force on the panel is calculated from the panel area and normal. The total force and moment are integrated by summing up the panel forces (Matusiak, 2013).

The radiation force and moment are divided into an added mass part and a radiation-induced potential damping (Fossen, 2002; Perez, 2005)

$$\begin{Bmatrix} \mathbf{f}_{rad} \\ \boldsymbol{\tau}_{rad} \end{Bmatrix} = \begin{Bmatrix} \mathbf{f}_A \\ \boldsymbol{\tau}_A \end{Bmatrix} + \begin{Bmatrix} \mathbf{f}_P \\ \boldsymbol{\tau}_P \end{Bmatrix} . \tag{7}$$

The added mass part of the radiation forces and moments is dependent on the total ship acceleration including centripetal acceleration

$$\begin{Bmatrix} \mathbf{f}_A \\ \boldsymbol{\tau}_A \end{Bmatrix} = -\mathbf{M}_A \begin{Bmatrix} \dot{\mathbf{U}} \\ \dot{\mathbf{\Omega}} \end{Bmatrix} - \mathbf{C}_A(\mathbf{U}, \mathbf{\Omega}) \begin{Bmatrix} \mathbf{U} \\ \mathbf{\Omega} \end{Bmatrix} , \tag{8}$$

where the added mass matrix is

$$\mathbf{M}_A = \begin{bmatrix} \mathbf{A}_U & \mathbf{A}_{U\Omega} \\ \mathbf{A}_{\Omega U} & \mathbf{A}_\Omega \end{bmatrix} , \tag{9}$$

and the centripetal added mass matrix dependent on the ship velocities is

$$\mathbf{C}_A(\mathbf{U}, \mathbf{\Omega}) = \begin{bmatrix} \mathbf{0}_{3\times3} & -\mathbf{S}(\mathbf{A}_U\mathbf{U} + \mathbf{A}_{U\Omega}\mathbf{\Omega}) \\ -\mathbf{S}(\mathbf{A}_U\mathbf{U} + \mathbf{A}_{U\Omega}\mathbf{\Omega}) & -\mathbf{S}(\mathbf{A}_{\Omega U}\mathbf{U} + \mathbf{A}_\Omega\mathbf{\Omega}) \end{bmatrix} . \tag{10}$$

Radiation induced potential damping is

$$\begin{Bmatrix} \mathbf{f}_P \\ \boldsymbol{\tau}_P \end{Bmatrix} = -\mathbf{B}_A \begin{Bmatrix} \mathbf{U} \\ \mathbf{\Omega} \end{Bmatrix} , \tag{11}$$

where damping matrix is

$$\mathbf{B}_A = \begin{bmatrix} \mathbf{B}_U & \mathbf{B}_{U\Omega} \\ \mathbf{B}_{\Omega U} & \mathbf{B}_\Omega \end{bmatrix} . \tag{12}$$

When the gravity-, hydrostatic and radiation forces are plugged to the ship equation of motion (Equation 3) the equation becomes

$$\mathbf{M} \begin{Bmatrix} \dot{\mathbf{U}} \\ \dot{\mathbf{\Omega}} \end{Bmatrix} + [\mathbf{C}(\mathbf{U}, \mathbf{\Omega}) + \mathbf{B}_A] \begin{Bmatrix} \mathbf{U} \\ \mathbf{\Omega} \end{Bmatrix} = \begin{Bmatrix} \mathbf{f}_g \\ \mathbf{0}_{3\times1} \end{Bmatrix} + \begin{Bmatrix} \mathbf{f}_H(\mathbf{R}, \mathbf{\Theta}) \\ \boldsymbol{\tau}_H(\mathbf{R}, \mathbf{\Theta}) \end{Bmatrix} , \tag{13}$$

where $\mathbf{M}$ and $\mathbf{C}(\mathbf{U}, \mathbf{\Omega})$ are generalized mass- and centripetal mass matrices containing the ship inertia and added mass properties.

Added mass and damping matrices are assumed to be constant during the simulation. Added mass and damping values are calculated with the linear strip method (Salvesen et al., 1970). The applied computational code is based on the SEALOADS code presented by Meyers et al. (1975). The added mass and damping values for each strip are calculated applying two-dimensional source distribution Frank (1967) method. Vassalos and Jasionowski (2002) show the complexity of estimating the hydrodynamic coefficients for damaged ship around high roll angles, thus constant added mass and damping values at the ship natural motion frequencies are applied. his assumption of constant added mass and damping terms neglects the effect of high roll angles and the increase in draft. The variation in the motion frequencies is also not accounted for.

3. Model for the flooding process

The floodwater motions are modelled with the lumped mass method with a moving free surface (Jasionowski, 2001; Spanos and Papanikolaou, 2001; Valanto, 2008). The variation of the mass is accounted for in the model. In the ITTC (2014) the equation of change of the momentum is written for the ship, while here the equation is written for the lumped mass. Change of the inertia due to the floodwater is coupled to the ship motions through the coupled equations of motions treated in section 4. The lumped mass model assumes a plane surface in the flooded room. Position of the lumped mass is calculated as a function of surface angle and floodwater volume in the room from the geometry of the floodwater.

The flow through the opening is modelled with the hydraulic model based

on Bernoulli equation. In/outflow jet i.e. the inflow momentum flux is accounted for as a force acting on the lumped mass. Energy dissipation in the motion of the floodwater due to the viscous effects is modelled as a friction force acting on the lumped mass. In the following subsections detailed descriptions of applied models for the flooding process are given.

3.1. Equation of motion for the lumped mass

The lumped mass m_i is treated as a rigid point mass. Starting from the conservation of momentum, equation of translational motion for the lumped mass, written in the inertial coordinate system **XYZ** is

$$\begin{aligned} \frac{D}{Dt}\left(m_i\dot{\mathbf{R}}_i\right) &= \mathbf{F}_{tot,i} \\ m_i\ddot{\mathbf{R}}_i + \dot{m}_i\dot{\mathbf{R}}_i &= \mathbf{F}_{tot,i}, \end{aligned} \tag{14}$$

where $\mathbf{R}_i$ is lumped mass position in the inertial coordinate system and $\mathbf{F}_{tot,i}$ is the total force acting on the lumped mass. The lumped mass position is then expressed as $\mathbf{R}_i = \mathbf{R} + \mathbf{r}_i$, where $\mathbf{r}_i$ is the lumped mass position with respect to the ship coordinate system. The time derivatives of the lumped mass position are

$$\begin{aligned} \dot{\mathbf{R}}_i &= \mathbf{U} - S(\mathbf{r}_i)\boldsymbol{\Omega} + \mathbf{v}_i \\ \ddot{\mathbf{R}}_i &= \dot{\mathbf{U}} - S(\mathbf{r}_i)\dot{\boldsymbol{\Omega}} + \dot{\mathbf{v}}_i + S(\boldsymbol{\Omega})\mathbf{U} - S(\boldsymbol{\Omega})S(\mathbf{r}_i)\boldsymbol{\Omega} + 2S(\boldsymbol{\Omega})\mathbf{v}_i\,, \end{aligned} \tag{15}$$

where $\mathbf{v}_i$ is lumped mass velocity with respect to the ship fixed coordinate system **xyz**. Following equation of translational motion for the lumped mass in the ship fixed coordinate system is obtained by inserting the time deriva-

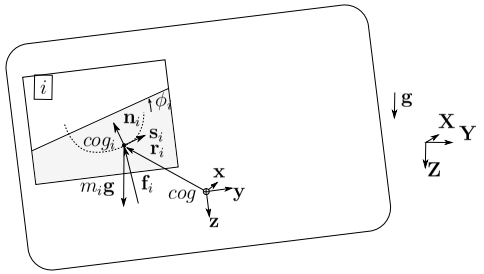

Figure 2: 2D model for lumped mass motions.

tives of $\mathbf{R}_i$ into Equation 14

$$m_i\Big[\dot{\mathbf{U}} - S(\mathbf{r}_i)\dot{\mathbf{\Omega}} + \dot{\mathbf{v}}_i + S(\mathbf{\Omega})\mathbf{U} - S(\mathbf{\Omega})S(\mathbf{r}_i)\mathbf{\Omega} + 2S(\mathbf{\Omega})\mathbf{v}_i\Big] + \dot{m}_i\Big[\mathbf{U} - S(\mathbf{r}_i)\mathbf{\Omega} + \mathbf{v}_i\Big] = \mathbf{f}_{g,i} + \mathbf{f}_{\dot{m},i} + \mathbf{f}_i \ , \qquad (16)$$

where the total force acting on the lumped mass is divided into the gravity force vector $\mathbf{f}_{g,i}(\mathbf{\Theta}) = m_i\mathbf{g}(\mathbf{\Theta})$, the inflow momentum-flux $\mathbf{f}_{\dot{m},i}$ and to the force ship is exerting on the lumped mass $\mathbf{f}_i$.

The lumped mass position is limited to a path of possible locations of floodwater center of gravity cog_i (Figure 2). The position of the lumped mass $\mathbf{r}_i(\phi, V_i)$ is a function of surface angle ϕ_i and volume $V_i = m_i/\rho$ (or mass m_i). An assumption, that the surface angle does not change as the mass varies, is made. Thus the derivatives of $\mathbf{r}_i$ with respect to time are $\dot{\mathbf{r}}_i = \mathbf{v}_i = \dot{\phi}_i\mathbf{r}_{i,\phi_i}$ and $\ddot{\mathbf{r}}_i = \ddot{\phi}_i\mathbf{r}_{i,\phi_i} + \dot{\phi}_i^{\,2}\mathbf{r}_{i,\phi_i\phi_i}$, where suffix $_{\phi_i}$ denote partial derivative with respect to the surface angle. The terms related to the mass variation were omitted above. This means that the lumped mass moves in the direction perpendicular to the surface normal as defined in Spanos and Papanikolaou (2001) and Jasionowski (2001) (i.e. in a path defined by a constant mass) and as the mass varies the path is updated accordingly. Inserting the derivatives of the lumped mass location vector to the translational equation of motion for the lumped mass (Equation 16) an equation of motion for lumped mass angle is obtained (Manderbacka et al., 2014b)

$$m_i\Big[\dot{\mathbf{U}} - S(\mathbf{r}_i)\dot{\mathbf{\Omega}} + \ddot{\phi}_i\mathbf{r}_{i,\phi_i} + \dot{\phi}_i^{\,2}\mathbf{r}_{i,\phi_i\phi_i} + S(\mathbf{\Omega})\mathbf{U} - S(\mathbf{\Omega})S(\mathbf{r}_i)\mathbf{\Omega} + 2S(\mathbf{\Omega})\dot{\phi}_i\mathbf{r}_{i,\phi_i}\Big] + \dot{m}_i\Big[\mathbf{U} - S(\mathbf{r}_i)\mathbf{\Omega} + \dot{\phi}_i\mathbf{r}_{i,\phi_i}\Big] = \mathbf{f}_{g,i} + \mathbf{f}_{\dot{m},i} + \mathbf{f}_i \ . \qquad (17)$$

The force ship exerts on the mass depends on the model of interaction between the lumped mass and the ship. In this work the force $\mathbf{f}_i$ acting on the lumped mass is modelled as a sum of support force and friction i.e the viscous forces or dissipative forces. Support force $\mathbf{f}_{n,i}$ acts along the direction normal to the lumped mass path (Figure 2). Friction force $\mathbf{f}_{k,i}$ acts along the tangent direction of the lump mass path

$$\mathbf{f}_i = \mathbf{f}_{n,i} + \mathbf{f}_{k,i} \ . \qquad (18)$$

Multiplying the force vector $\mathbf{f}_i$ by the tangent vector of the surface $\mathbf{s}_i = \frac{\mathbf{r}_{i,\phi_i}}{|\mathbf{r}_{i,\phi_i}|}$ eliminates the support force and yields the scalar value of the friction force $f_{k,i}$ in the direction of the path

$$\begin{aligned} \mathbf{f}_i \cdot \mathbf{s}_i &= \mathbf{f}_{n,i} \cdot \mathbf{s}_i + \mathbf{f}_{k,i} \cdot \mathbf{s}_i \\ &= 0 + f_{k,i} \ . \end{aligned} \qquad (19)$$

3.2. Energy dissipation friction model

Energy dissipation can be modelled as viscous linear damping (Silverman and Abrahamson, 1966) in equivalent mechanical models for sloshing (Dodge, 1966). In the pendulum model for sloshing presented by Godderidge et al. (2012) linear and nonlinear dissipation models have been applied. In this work linear viscous damping model is used. The viscous forces are modelled with a friction model. Friction force vector is acting on the opposite direction of the lumped mass velocity

$$\begin{aligned} f_{k,i} &= \mathbf{f}_{k,i} \cdot \mathbf{s}_i \\ &= -\delta_i m_i \mathbf{v}_i \cdot \mathbf{s}_i \\ &= -\delta_i m_i \dot{\phi}_i \mathbf{r}_{i,\phi_i} \cdot \frac{\mathbf{r}_{i,\phi_i}}{|\mathbf{r}_{i,\phi_i}|} \\ &= -\delta_i m_i \dot{\phi}_i |\mathbf{r}_{i,\phi_i}| \,, \end{aligned} \tag{20}$$

where δ_i is friction coefficient for floodwater i. The evaluation of the friction coefficient is based on a model for the dissipation of the energy of standing waves in rectangular rooms (Keulegan, 1959). Viscous dissipation on the walls and the floor of a rectangular room with length l and breadth b is estimated by

$$\delta = \frac{kg\pi}{\omega^2 \cosh(kh)^2} \sqrt{\frac{\mu}{2\rho\omega}} \left(\sinh(2kh) + lk(\sinh(2kh) - 2kh) + lk \right) , \tag{21}$$

where $k = \pi/b$ is the wave number, $\omega = \sqrt{g\pi/b \tanh(\pi h/b)}$ is the natural frequency of the sloshing, h is the average height of the fluid in the room, μ is dynamic viscosity, ρ is the fluid density.

3.3. Water flow through the opening

The flow through the opening is calculated using hydraulic equation. This approach has been validated by model tests for water exchange between the floodwater through non-watertight openings in a harmonic motion of the room (Manderbacka et al., 2014a). For tall openings the flow velocity at different positions of the opening is calculated according to the pressures at these position and the flow rate obtained by integration over the opening height (Dillingham, 1981; Ruponen, 2007).

Flow through a tall opening that extends from the position A to D is calculated in parts; from the opening bottom to the lower water level AB and from the lower water level to the higher water level BC, (Figure 3). The pressures on both sides of the opening (p_j and p_i) are evaluated at the positions A, B, C and D. If the lower water level is below the opening then B=A and if the upper level is also below the opening then C=B=A. If higher water level is above the opening then C=D and if also the lower water level is above the opening then C=B=D. Pressure at water surface is set to air pressure, here zero. This means that the model assumes fully ventilated rooms. Air flow or compressibility is not taken into account. Pressure between the positions A, B and C is assumed to vary linearly. The position at the opening is described by a variable s describing the position along the height of the opening. Flow velocity from room j into the room i at position s at the opening is evaluated by applying hydraulic equation

$$v_{ij}(s) = C_{d,ij} sign\left(\Delta p(s)\right) \sqrt{\frac{2}{\rho} |\Delta p(s)|} \,. \tag{22}$$

where the $C_{d,ij}$ is the discharge coefficient of the opening between the room i and j and $\Delta p(s) = p_j(s) - p_i(s)$ is the pressure difference between the rooms

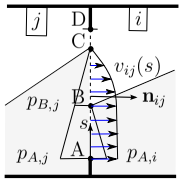

Figure 3: Flow rate calculation.

at height s in the opening. The linear variation of the pressure difference between the positions A, B and C can be written as

$$\Delta p(s) = \frac{\Delta p_B - \Delta p_A}{s_B - s_A}(s - s_A) + \Delta p_A \quad \text{when } A < s < B$$
$$\Delta p(s) = \frac{\Delta p_C - \Delta p_B}{s_C - s_B}(s - s_B) + \Delta p_C \quad \text{when } B < s < C. \tag{23}$$

The total flow rate is integrated in parts AB and BC over the opening height from the Equation 22. It can be shown that if the $sign(\Delta p(s))$ does not change between the s_A and s_B (i.e. $0 < \Delta p_A \cdot \Delta p_B$), the integral results in

$$\begin{aligned} Q_{AB} &= \int_{s_A}^{s_B} v_{ij}(s) b_{ij}\, ds \\ &= C_{d,ij} b_{ij}\, sign\left(\Delta p(s)\right) \int_{s_A}^{s_B} \sqrt{\frac{2}{\rho}|\Delta p(s)|}\, ds \\ &= C_{d,ij} b_{ij} \frac{2}{3}\sqrt{\frac{2}{\rho}}\, \frac{s_B - s_A}{\Delta p_B - \Delta p_A}\left[|\Delta p_B|^{3/2} - |\Delta p_A|^{3/2}\right] \end{aligned} \tag{24}$$

where b_{ij} is the breadth of the opening and ds is an infinitesimal variation in the height along the opening. When $\Delta p_A \to \Delta p_B$ then $Q_{AB} = C_{d,ij} b_{ij}\, sign\left(\Delta p_A\right) \sqrt{\frac{2}{\rho}|\Delta p_A|}(s_B - s_A)$. If $sign(\Delta p(s))$ change between the s_A

and s_B (i.e. $0 > \Delta p_A \cdot \Delta p_B$) then

$$\begin{aligned} Q_{AB} = C_{d,ij} b_{ij} \frac{2}{3}\sqrt{\frac{2}{\rho}} \Big[& sign\left(\Delta p_A\right)\left(s_0 - s_A\right)\sqrt{|\Delta p_A|} \\ & + sign\left(\Delta p_B\right)\left(s_B - s_0\right)\sqrt{|\Delta p_B|}\Big] , \end{aligned} \tag{25}$$

where s_0 is the point where the sign of the Δp changes (i.e. $\Delta p(s_0) = 0$). Similarly, as above, for the part BC. The flow rate through the opening from room j to room i is then the sum of the flow rates at the parts AB and BC

$$Q_{ij} = Q_{AB} + Q_{BC} \ . \tag{26}$$

Finally the mass variation in room i is calculated by summing up flow rate through all the openings connected to it

$$\dot{m}_i = \rho Q_i = \rho \sum_{j=1}^{n_{i,o}} Q_{ij} \ , \tag{27}$$

where $n_{i,o}$ is the number of the openings connected to room i.

3.4. In/outflow momentum flux

Momentum flux through the opening ij is integrated over the opening height s from the bottom of the opening s_A to the top of the opening s_D

$$\begin{aligned} \mathbf{f}_{\dot{m},ij} &= \int_{s_A}^{s_D} d\dot{m}_{ij}(s)\ \mathbf{v}_{ij}(s) \\ &= \int_{s_A}^{s_D} d\dot{m}_{ij}(s)\ v_{ij}(s)\ \mathbf{n}_{ij} \ , \end{aligned} \tag{28}$$

where $d\dot{m}_{ij} = \rho\ dQ_{ij}(s) = \rho\ v_{ij}(s)\ b_{ij}\ ds$ is the mass flow through an infinitesimally high slice of opening and $\mathbf{n}_{ij}$ is vector pointing from the room j into the room i (Figure 3)

$$\mathbf{f}_{\dot{m},ij} = \int_{s_A}^{s_D} \rho\ v_{ij}(s)^2\ b_{ij}\ ds\ \mathbf{n}_{ij} \ . \tag{29}$$

Force acting on the fluid in the room i points always in the direction of the normal (inside the room) regardless of the flow direction. If the flow is positive into the room the inflooding flow adds momentum in the direction of the flow. If the flow is negative outflooding acts as a jet outburst causing a force pointing into the room. The velocity as a function of s is obtained from the Equations 22 and 23. The momentum flux is integrated in parts AB and BC over the opening height

$$\mathbf{f}_{\dot{m},AB} = C_{d,ij}^2 b_{ij} |\Delta p_B + \Delta p_A| (s_B - s_A) \mathbf{n}_{ij} \tag{30}$$

and similarly for the part BC. The total momentum flux through the opening ij is

$$\mathbf{f}_{\dot{m},ij} = \mathbf{f}_{\dot{m},AB} + \mathbf{f}_{\dot{m},BC} \ . \tag{31}$$

Finally the momentum flux to the room i is the sum of the momentum fluxes through all openings connected to the room

$$\mathbf{f}_{\dot{m},i} = \sum_{j=1}^{n_{i,o}} \mathbf{f}_{\dot{m},ij} \ . \tag{32}$$

4. Coupled ship and floodwater model

The equations of motion for the ship (Equation 13) and the for lumped mass (Equation 17) can be combined and written in a matrix form. The ship exerts a force $\mathbf{f}_i$ to the lumped mass. The force-moment vector that the lumped mass exerts on the ship is $\{-\mathbf{f}_i, \ -\mathbf{r}_i \times \mathbf{f}_i\}^T$.

The combined equations of motion are

$$\begin{aligned}
&\begin{bmatrix} \mathbf{M}_{11} & \mathbf{M}_{12} & \mathbf{0}_{3\times1} \\ \mathbf{M}_{21} & \mathbf{M}_{22} & \mathbf{0}_{3\times1} \\ m_i\mathbf{I}_{3\times3} & -m_i\mathbf{S}(\mathbf{r}_i) & m_i\mathbf{r}_{i,\phi_i} \end{bmatrix} \begin{Bmatrix} \dot{\mathbf{U}} \\ \dot{\mathbf{\Omega}} \\ \ddot{\phi}_i \end{Bmatrix} \\
+ &\left(\begin{bmatrix} \mathbf{C}_{11}(\mathbf{U},\mathbf{\Omega}) & \mathbf{C}_{12}(\mathbf{U},\mathbf{\Omega}) & \mathbf{0}_{3\times1} \\ \mathbf{C}_{21}(\mathbf{U},\mathbf{\Omega}) & \mathbf{C}_{22}(\mathbf{U},\mathbf{\Omega}) & \mathbf{0}_{3\times1} \\ m_i\mathbf{S}(\mathbf{\Omega}) & -m_i\mathbf{S}(\mathbf{\Omega})\mathbf{S}(\mathbf{r}_i) & m_i\Big(2\mathbf{S}(\mathbf{\Omega})\mathbf{r}_{i,\phi_i} + \dot{\phi}_i\mathbf{r}_{i,\phi_i\phi_i}\Big) \end{bmatrix} \right. \\
+ &\left. \begin{bmatrix} \mathbf{B}_{11} & \mathbf{B}_{12} & \mathbf{0}_{3\times1} \\ \mathbf{B}_{21} & \mathbf{B}_{22} & \mathbf{0}_{3\times1} \\ \mathbf{0}_{3\times3} & \mathbf{0}_{3\times3} & \mathbf{0}_{3\times1} \end{bmatrix} + \begin{bmatrix} \mathbf{0}_{3\times3} & \mathbf{0}_{3\times3} & \mathbf{0}_{3\times1} \\ \mathbf{0}_{3\times3} & \mathbf{0}_{3\times3} & \mathbf{0}_{3\times1} \\ \dot{m}_i\mathbf{I}_{3\times3} & -\dot{m}_i\mathbf{S}(\mathbf{r}_i) & \dot{m}_i\mathbf{r}_{i,\phi_i} \end{bmatrix} \right) \begin{Bmatrix} \mathbf{U} \\ \mathbf{\Omega} \\ \dot{\phi}_i \end{Bmatrix} \\
= &\begin{Bmatrix} \mathbf{f}_g(\mathbf{\Theta}) \\ \mathbf{0}_{3\times1} \\ \mathbf{0}_{3\times1} \end{Bmatrix} + \begin{Bmatrix} \mathbf{f}_H(\mathbf{R},\mathbf{\Theta}) \\ \mathbf{T}_H(\mathbf{R},\mathbf{\Theta}) \\ \mathbf{0}_{3\times1} \end{Bmatrix} + \begin{Bmatrix} \mathbf{0}_{3\times1} \\ \mathbf{0}_{3\times1} \\ \mathbf{f}_{g,i}(\mathbf{\Theta}) \end{Bmatrix} + \begin{Bmatrix} \mathbf{0}_{3\times1} \\ \mathbf{0}_{3\times1} \\ \mathbf{f}_{\dot{m},i} \end{Bmatrix} \\
+ &\begin{Bmatrix} -\mathbf{f}_i \\ -\mathbf{S}(\mathbf{r}_i)\mathbf{f}_i \\ \mathbf{f}_i \end{Bmatrix} \ .
\end{aligned} \tag{33}$$

Interaction force vector $\mathbf{f}_i$ is eliminated from the combined equation of motion matrix rows related to the ship translational and angular motion by summing the lumped mass equation of motion on them. Finally the lumped mass equation of motion is multiplied by the tangent vector of the lumped mass path to eliminate the normal force acting on the lumped mass (see

subsection 3.1). The system equation of motion can be written as

$$\left[\mathbf{M}+\mathbf{M}_i\right]\begin{Bmatrix}\dot{\mathbf{U}}\\ \dot{\mathbf{\Omega}}\\ \ddot{\phi}_i\end{Bmatrix}+\left[\mathbf{C}(\mathbf{U},\mathbf{\Omega})+\mathbf{B}_A+\mathbf{C}_i(\mathbf{\Omega},\dot{\phi}_i,\mathbf{r}_i)+\dot{\mathbf{M}}_{\dot{m}_i,i}\right]\begin{Bmatrix}\mathbf{U}\\ \mathbf{\Omega}\\ \dot{\phi}_i\end{Bmatrix}$$
$$=\mathbf{F}_g(\mathbf{\Theta})+\mathbf{F}_H(\mathbf{R},\mathbf{\Theta})+\mathbf{F}_{g,i}(\mathbf{\Theta})+\mathbf{F}_{\dot{m},i}+\mathbf{F}_{k,i}\ , \quad (34)$$

where the contribution of the floodwater is divided into the following terms; lumped mass generalized mass matrix

$$\mathbf{M}_i=m_i\begin{bmatrix}\mathbf{I}_{3\times3} & -\mathbf{S}(\mathbf{r}_i) & \mathbf{r}_{i,\phi_i}\\ \mathbf{S}(\mathbf{r}_i) & -\mathbf{S}(\mathbf{r}_i)^2 & \mathbf{S}(\mathbf{r}_i)\mathbf{r}_{i,\phi_i}\\ \mathbf{r}_{i,\phi_i}^T & -\mathbf{r}_{i,\phi_i}^T\mathbf{S}(\mathbf{r}_i) & \mathbf{r}_{i,\phi_i}^T\mathbf{r}_{i,\phi_i}\end{bmatrix}\ , \quad (35)$$

lumped mass centripetal mass matrix

$$\mathbf{C}_i=m_i\begin{bmatrix}\mathbf{S}(\mathbf{\Omega}) & -\mathbf{S}(\mathbf{\Omega})\mathbf{S}(\mathbf{r}_i) & \left(2\mathbf{S}(\mathbf{\Omega})\mathbf{r}_{i,\phi_i}+\dot{\phi}_i\mathbf{r}_{i,\phi_i\phi_i}\right)\\ \mathbf{S}(\mathbf{r}_i)\mathbf{S}(\mathbf{\Omega}) & -\mathbf{S}(\mathbf{r}_i)\mathbf{S}(\mathbf{\Omega})\mathbf{S}(\mathbf{r}_i) & \mathbf{S}(\mathbf{r}_i)\left(2\mathbf{S}(\mathbf{\Omega})\mathbf{r}_{i,\phi_i}+\dot{\phi}_i\mathbf{r}_{i,\phi_i\phi_i}\right)\\ \mathbf{r}_{i,\phi_i}^T\mathbf{S}(\mathbf{\Omega}) & -\mathbf{r}_{i,\phi_i}^T\mathbf{S}(\mathbf{\Omega})\mathbf{S}(\mathbf{r}_i) & \mathbf{r}_{i,\phi_i}^T\left(2\mathbf{S}(\mathbf{\Omega})\mathbf{r}_{i,\phi_i}+\dot{\phi}_i\mathbf{r}_{i,\phi_i\phi_i}\right)\end{bmatrix}\ , \quad (36)$$

lumped mass rate of mass change matrix

$$\dot{\mathbf{M}}_{\dot{m}_i,i}=\frac{\dot{m}_i}{m_i}\mathbf{M}_i\ , \quad (37)$$

lumped mass gravitation force vector

$$\mathbf{F}_{g,i}=\begin{Bmatrix}I_{3\times3}\\ \mathbf{S}(\mathbf{r}_i)\\ \mathbf{r}_{i,\phi_i}^T\end{Bmatrix}m_i\mathbf{g}(\mathbf{\Theta})\ , \quad (38)$$

lumped mass inflow/outflow momentum-flux force vector

$$\mathbf{F}_{\dot{m},i}=\begin{Bmatrix}I_{3\times3}\\ \mathbf{S}(\mathbf{r}_i)\\ \mathbf{r}_{i,\phi_i}^T\end{Bmatrix}\mathbf{f}_{\dot{m},i}\ , \quad (39)$$

where $\mathbf{f}_{\dot{m},i}$ is calculated accoring to the Equation 32. Lumped mass friction vector is

$$\mathbf{F}_{k,i}=\begin{Bmatrix}\mathbf{0}_{3\times1}\\ \mathbf{0}_{3\times1}\\ |\mathbf{r}_{i,\phi_i}|f_{k,i}\end{Bmatrix}\ , \quad (40)$$

where $f_{k,i}$ is calculated applying Equation 20.

4.1. Implementation of the time domain simulation

Ship and floodwater modelled with a moving lumped mass constitutes a multi-body system where the lumped masses vary in time. The system state vector $\boldsymbol{\chi}=\left\{\mathbf{U},\mathbf{\Omega},\dot{\phi}_i,m_i,\mathbf{R},\mathbf{\Theta},\phi_i\right\}^T$ consists of the ship velocities in the ship fixed coordinate system (translational and angular), floodwater free surface angle rate of change in each flooded room, floodwater mass in each room, ship position in the inertial coordinate system (translational and angular) and floodwater free surface angle. The vector describes the system state at each time step unambiguously. The numerical simulation in time is performed by integrating the system state derivative with respect to time applying fourth order Runge-Kutta integration. System state derivative (ship accelerations, floodwater surface angular acceleration and mass rate of change) $d\boldsymbol{\chi}/dt=\left\{\dot{\mathbf{U}},\dot{\mathbf{\Omega}},\ddot{\phi}_i,\dot{m}_i,\dot{\mathbf{R}},\dot{\mathbf{\Theta}},\dot{\phi}_i\right\}^T$ is solved applying the models presented above. Ship acceleration and floodwater free surface angular acceleration are solved by applying the coupled ship and floodwater equation

of motion Equation 34. Combined equation of motion is multiplied with the inverse matrix of $[\mathbf{M} + \mathbf{M}_i]$ in order to solve for the accelerations. Floodwater mass may go to zero in the room. If mass m_i is smaller than a limit m_l then the equation corresponding to the room i in the combined set of equations is eliminated in order to have the total generalized mass matrix non-singular. The elimination is done with the boundary conditions setting value in the mass matrix to 1 and other values on the row and column i to zero. Mass rate of change is solved from the Equation 27. The derivative of the ship position in the inertial coordinate frame $\dot{\mathbf{R}} = \mathbf{T}(\boldsymbol{\Theta})\mathbf{U}$ is calculated by multiplying the velocities expressed in the ship fixed coordinate frame with a transformation matrix $\mathbf{T}(\boldsymbol{\Theta})$ from ship fixed coordinate system to inertial coordinate system. The derivative of the Euler angles $\dot{\boldsymbol{\Theta}} = \mathbf{T}_\Theta(\boldsymbol{\Theta})\boldsymbol{\Omega}$ is calculated by multiplying the angular velocities expressed in the ship fixed coordinate system with transformation matrix $\mathbf{T}_\Theta(\boldsymbol{\Theta})$ from the ship fixed angular velocities to the Euler angles.

Floodwater center of gravity is evaluated from the analytical equations as a function of volume (mass) and surface angle. The assumption of plane surface neglects the detailed effects of surface waves in the room but models the lowest natural sloshing motion close to the actual sloshing frequency (Jasionowski, 2001).

5. Setup for validation cases

The presented numerical model is validated against the experimental data of the box shaped barge transient flooding test presented by Manderbacka et al. (20xx). The box shaped barge is the same model as the one used

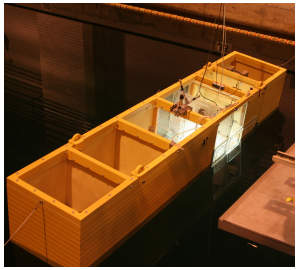

(a) Model in tank.

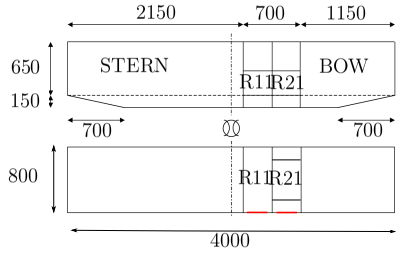

(b) Overall dimensions of the model and compartment locations.

Figure 4: Box-shaped-barge model (Manderbacka et al., 20xx).

in the ITTC benchmark study for the progressive flooding (van Walree and Papanikolaou, 2007). In the transient flooding tests the load case and the openings were modified compared to the progressive flooding tests (Ruponen et al., 2007). Roll decay in both intact and flooded conditions was simulated. Simulations of roll decay in damage condition are used to validate the coupled model of ship and floodwater motions. Transient flooding cases were simulated in order to validate the models for the flooding process.

5.1. Barge geometry

Simulations for the damaged box shaped barge model shown in Figure 4a, were performed in model scale. Main particulars of the box shaped barge model are given in Table 1. Barge model has two different compartments (Figure 4b); the undivided compartment R11 and the divided compartment R21. Both compartments are 335 mm long and 300 mm high. The undivided compartment R11 is 780 mm wide and it ranges over the barge breadth. Wall

thickness is 10 mm. The divided compartment R21 has two non-watertight longitudinal bulkheads with openings. The openings are 20 mm wide and 200 mm high and they are located at 5 mm height from the compartment bottom in the middle of the non-watertight bulkhead. The divided compartment is symmetrical with respect to the model center line. The middle room of the compartment is 460 mm wide. The rooms on the sides are 150 mm wide.

The damage openings to the compartments R11 and R21 are located at the starboard side in the middle of the compartment external wall. The damage opening size is 200 mm × 200 mm and it is located 50 mm above the compartment bottom. The damage opening was closed by a plate before the test. The plate was pulled aftwards to initiate the damage to compartment R11 and forwards for damage to compartment R21 by a radio controlled spring system. The opening time was estimated to be approximately 0.1 s or faster. This is considered as immediate opening in the simulations taking into account the time scale of the transient flooding. More detailed description of the model geometry and experiment arrangement is given by Manderbacka et al. (20xx).

The barge hull is represented by 4680 triangular panels in the simulation. Upper part of the barge hull, which does not get in touch with water, is not included in the panel model. Panel center points, areas and normals are calculated and used in the simulation. The center points of the panels are shown in Figure 5. Compartments R11 and R21 are modelled as two-dimensional compartments. The compartments in the simulation are located at each compartment longitudinal center. Floodwater motions in the longitudinal

Table 1: Model main particulars for two different initial metacentric heights.

	$\overline{GM}_{0,1}$	$\overline{GM}_{0,2}$
Length, L	4.000 m	
Breadth, B	0.800 m	
Draft, T	0.253 m	
Total mass, m	657 kg	
Initial metacentric height, $\overline{GM}_0$	0.0189 m	0.0274 m
cog height from keel, $\overline{KG}_0$	0.385 m	0.377 m
Roll moment of inertia, I_{xx}	80.9 kg m^2	79.2 kg m^2
Damage opening length × height	200 mm × 200 mm	
Damage opening height from the compartment bottom	50 mm	
R21 internal opening length × height	20 mm × 200 mm	
R21 internal opening height from the compartment bottom	5 mm	

x-direction are not modelled.

5.2. Simulation cases

All the cases were simulated at two different initial stabilities $\overline{GM}_{0,1}$ and $\overline{GM}_{0,2}$. In the simulation the values given in Table 1 were used for the ship inertia. The mass was set to value $m = 656$ (one kg less than in the measurements, since the bilge keels were not modelled in the panel model) and the rotational moment of inertia around the x-axis was taken from the measurements. For the rotational moment of inertia around y- and z-axes $I_{xx} = I_{yy} = m(L/4)^2 = 656$ kg m^2 was used. The off-diagonal terms in

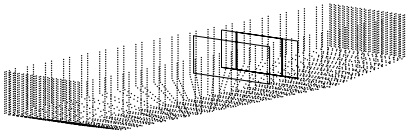

Figure 5: Panel center points and 2D representation of compartments R11 and R21.

the ship rotational inertia matrix $\mathbf{I}_S$ were set to zero. Simulations were performed for flooded undivided compartment R11 and for flooded divided compartment R21 shown in Figure 4.

The bilge keel damping was accounted for in the calculation of the added mass and damping in frequency domain with the potential strip code. The calculated values of the added mass and damping at the natural ship motion frequencies are taken for the time domain simulation. For the heave component 44 and the heave-pitch component 35 the added mass and damping value at the heave natural frequency is applied. For the roll 44, the roll-sway 24, the sway 22 and the roll-heave 46 components the values at natural roll frequency are applied. For the pitch 55 component the value at natural pitch frequency is applied. For the other calculated components; surge 11, sway-yaw 26 and yaw 66, the average values are applied. The added mass and the damping were calculated in the potential code coordinate frame located at the free water surface. They were then transferred to the ship coordinate frame where the origin is located at ship *cog* (Matusiak, 2013).

The added mass term for roll $M_{A,44}$ and the damping term for roll $B_{A,44}$ were adjusted according to the intact roll decay model test results. The

added mass term for roll was increased by 1.9 kg m^2 and the damping term was increased by 7.8 kg m^2/s in order to properly account for the effects of the bilge keels. The adjusted values are shown in the matrices below.

The values of the added mass and damping that were used in the simulation for the lower initial stability $\overline{GM}_{0,1}$ are

$$\mathbf{M}_{A,1} = \begin{bmatrix} 12.8 & 0 & 0 & 0 & 1.69 & 0 \\ & 463 & 0 & -11.5 & 0 & 2.01 \\ & & 738 & 0 & 24.8 & 0 \\ & & & 10.19 & 0 & -0.403 \\ & sym & & & 987 & 0 \\ & & & & & 256 \end{bmatrix},$$

$$\mathbf{B}_{A,1} = \begin{bmatrix} 14.1 & 0 & 0 & 0 & 1.87 & 0 \\ & 5.21 & 0 & -0.048 & 0 & 5.13 \\ & & 2520 & 0 & 88.2 & 0 \\ & & & 7.8 & 0 & -0.678 \\ & sym & & & 3180 & 0 \\ & & & & & 1230 \end{bmatrix},$$

and for the higher initial stability $\overline{GM}_{0,2}$

$$\mathbf{M}_{A,2} = \begin{bmatrix} 12.8 & 0 & 0 & 0 & 1.58 & 0 \\ & 478 & 0 & -7.81 & 0 & 2.01 \\ & & 738 & 0 & 24.8 & 0 \\ & & & 10.05 & 0 & -0.393 \\ & sym & & & 986 & 0 \\ & & & & & 256 \end{bmatrix},$$

$$\mathbf{B}_{A,2} = \begin{bmatrix} 14.1 & 0 & 0 & 0 & 1.75 & 0 \\ & 15.3 & 0 & -0.032 & 0 & 5.13 \\ & & 2520 & 0 & 88.2 & 0 \\ & & & 7.8 & 0 & -0.635 \\ & sym & & & 3180 & 0 \\ & & & & & 1230 \end{bmatrix},$$

where the units for added mass matrix in the upper left block of size 3×3 corresponding to the matrix $\mathbf{A}_U$ of Equation 9 are kg. Units for added mass matrix in the upper right corner block corresponding to the matrix $\mathbf{A}_{U\Omega}$ are kg m. The units of the lower left corner block corresponding to the matrix $\mathbf{A}_\Omega$ of the added mass matrix are kg m^2. Similarly for the damping matrix the units at the upper left corner block of size 3×3 corresponding to the matrix $\mathbf{B}_U$ of Equation 12 are kg/s. The units in the upper right corner block corresponding to the matrix $\mathbf{B}_{\mathbf{U\Omega}}$ are kg m/s. The units in the lower right corner block corresponding to the matrix $\mathbf{B}_\Omega$ of the damping matrix are kg m^2/s.

Roll decay in flooded condition was simulated for different amounts of floodwater in the compartment. These simulations were performed for both

initial stabilities and for both compartments. Six different floodwater amount in the compartment were used; m_i = 2.5 kg, 5.0 kg, 10.0 kg, 15.0 kg, 20.0 kg and 25.0 kg. Initial roll angle was set equal to the initial roll angle in the measurements. Discharge coefficients for the openings were taken from the measurements. Value $C_d = 0.75$ was used for the internal openings in the compartment R21 and $C_d = 0.65$ was used for the external damage opening.

Transient abrupt flooding in calm water was simulated at both initial stabilities. Flooding into both compartments was simulated separately. The barge was initially set stationary to zero heel and trim angle at intact barge draft. All compartments were initially empty. Damage opening is introduced at zero time instant and flooding starts immediately. Barge is free to move in all six degrees of freedom.

The correct evaluation of the hydrostatics in the simulation code was checked by comparing the GZ-curves in flooded condition against the ones calculated by NAPA software (shown in Manderbacka et al. (20xx)). A good correspondence of the hydrostatics calculation was observed. The GZ-curves were calculated with six different amounts of floodwater in the compartment. The curves calculated with the presented simulation code are shown in Figure 6.

6. Results

Roll decay and transient flooding simulations were performed for the barge model in calm water. Roll decay simulations were performed in intact and flooded conditions. All the cases were simulated for undivided and divided compartment at two different initial stabilities. All the simulation

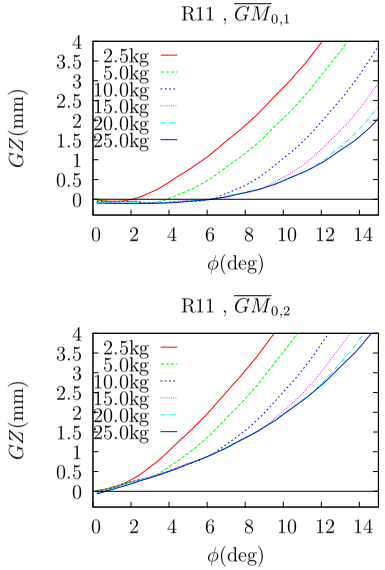

Figure 6: GZ curves for different water amounts for both initial stabilities calculated with presented simulation method.

time histories are compared against the measurement results presented in Manderbacka et al. (20xx).

Each case was simulated for 60 seconds. Time step in the simulations was 0.01 s. Simulation of 24 cases, i.e. 24 min of simulated time, took 30 min with a personal laptop with Intel Core i5-3210M 2.50GHz processor. Most of the calculation time is used on calculating the hydrostatic pressure at each panel. Simulations were performed in model scale, where the simulation time is nearly real time. The time step could be set $\sqrt{\lambda}$ (where λ is the scale) times bigger in full scale for the same amount of steps per roll period. The calculation time per time step is the same in full scale, thus in full scale the simulation would be faster than the real time.

6.1. Roll decay

Intact model roll decay simulation results are compared with the measurement results for both initial stabilities in Figure 7. With the presented adjusted values for the added mass matrix variable $M_{A,44}$ and the damping matrix variable $B_{A,44}$ the simulated roll damping for intact ship match well with the measurement time histories. It can be noted that the roll decay of the barge is not totally linear and thus towards the end of the time history the damping in the simulation is slightly bigger than the measured one.

The roll decay tests in flooded condition with constant amount of water were simulated for both initial stabilities ($\overline{GM}_{0,1}$ and $\overline{GM}_{0,2}$) and for both undivided (R11) and divided compartments (R21). Roll decay was simulated with six different amounts of floodwater. All together 24 cases of roll decay in flooded condition were simulated. Simulated roll is compared with the measured roll time histories. Simulations were performed with three different

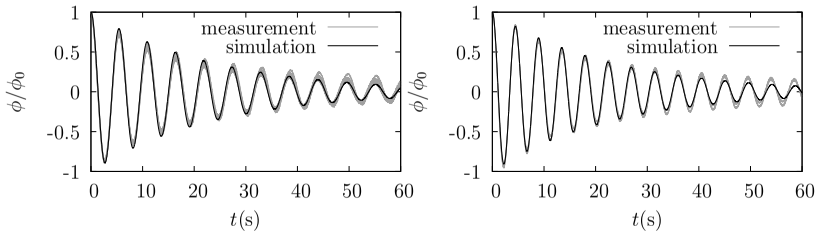

(a) $\overline{GM}_{0,1}$. (b) $\overline{GM}_{0,2}$.

Figure 7: Roll decay for intact model.

friction coefficients of the lumped mass motion. In addition to simulations with the friction coefficient estimated by Equation 21 the simulations were also performed without friction and with five times bigger friction factor than the estimated one. The results of roll decay in flooded condition are shown in Figure 8 for the undivided compartment R11 and in Figure 9 for the divided compartment R21.

The simulations with undivided compartment at higher initial stability (R11, $\overline{GM}_{0,2}$, Figure 8b) with fill amounts of 10.0 kg and higher, agree well with the measurements. The simulated roll decay results for the divided compartment R21 at both initial stabilities (Figure 8) also correspond well to the measurements. The simulations for the undivided compartment at lower initial stability (R11, $\overline{GM}_{0,1}$, Figure 8a) for the fill amounts of 15.0 kg and higher, have a longer second roll period than in the measurements. Otherwise, they decay in a same rate as in the measurements. In these above mentioned cases the friction coefficient has very little or hardly any impact.

In the simulations for the undivided compartment R11 at the lowest two fill amounts 2.5 kg and 5.0 kg the friction coefficient affect to the simulation results. At these fill amounts, simulations with the highest friction coefficient, give the best correspondence with the measurements.

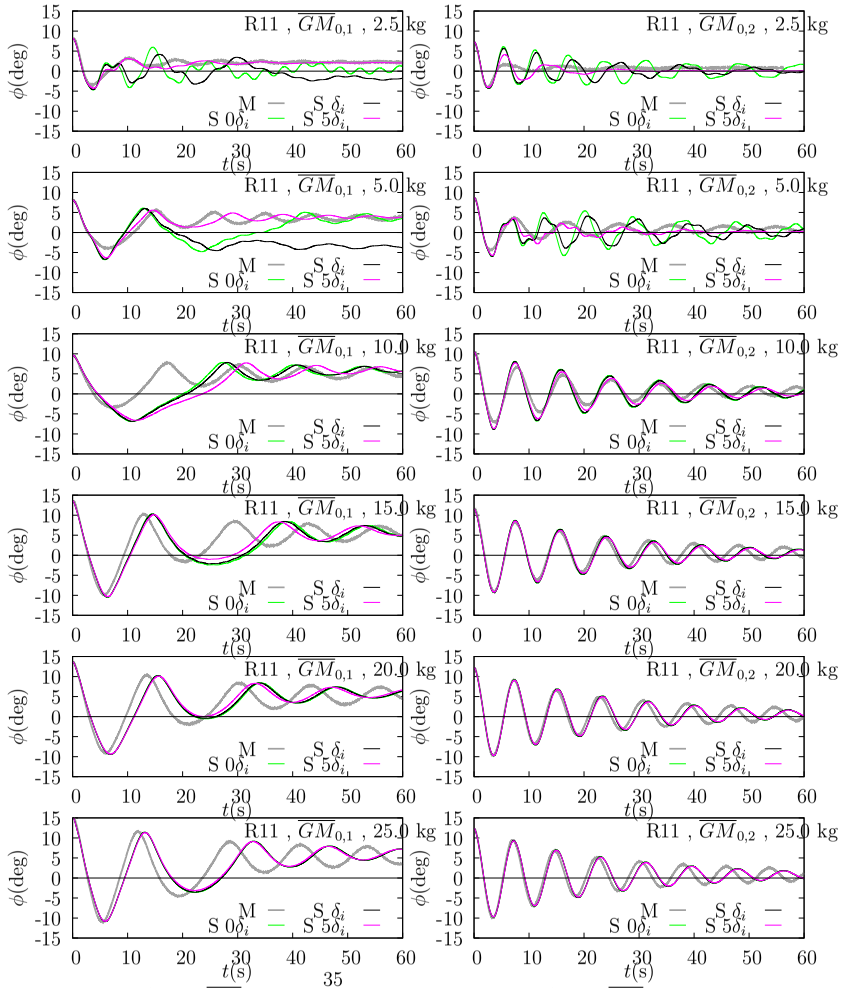

(a) R11, $\overline{GM}_{0,1}$. (b) R11, $\overline{GM}_{0,2}$.

Figure 8: Roll angle, roll decay tests with constant amount of floodwater in compartment R11. Measurement M, simulation without friction S $0\delta_i$, simulation with normal friction S δ_i and simulation with five time bigger friction S δ_i.

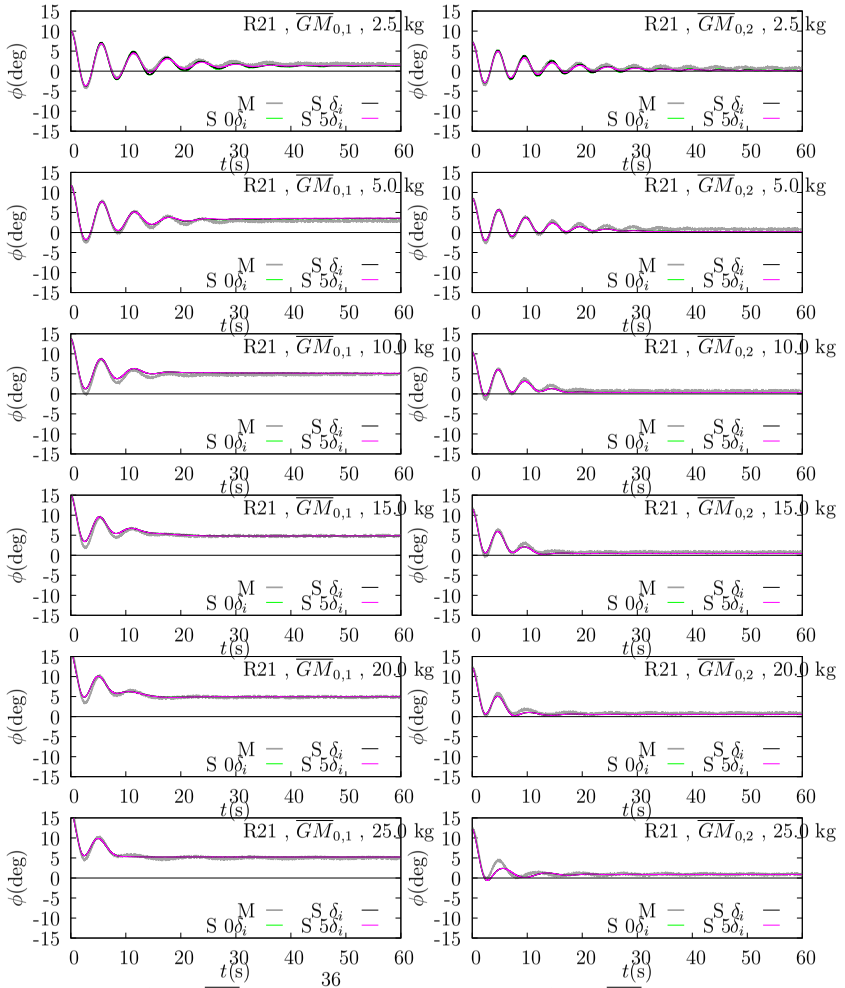

(a) R21, $\overline{GM}_{0,1}$. (b) R21, $\overline{GM}_{0,2}$.

Figure 9: Roll angle, roll decay tests with constant amount of floodwater in compartment R21. Measurement M, simulation without friction S $0\delta_i$, simulation with normal friction S δ_i and simulation with five time bigger friction S $5\delta_i$.

6.2. Transient flooding

Transient flooding was simulated with two different initial stabilities $\overline{GM}_{0,1}$ and $\overline{GM}_{0,2}$ for undivided compartment R11 and divided compartment R21 separately. The impact of the inflow momentum flux was studied by simulating all these four cases with and without the inflow momentum flux term Equation 32. Also the impact of the friction coefficient was studied by simulating the cases without the friction, with normal friction and with five times larger friction. Simulations are compared to the measured roll and draft increase. The roll accuracy in the measurements was ± 0.2 deg and accuracy in the draft increase data was ± 1 mm. For the undivided compartment the floodwater mass data is also available. The data of the water mass in the measurements was estimated by integrating the tracked surface elevation (Manderbacka et al., 20xx). The tracking of the surface from the videos was performed up to 30 seconds of the measurement record.

In the transient flooding experiments for the undivided compartment R11 the model heels approximately half a degree on the damage side right at the beginning of the flooding. The first large roll angle occurs onto the opposite side of the damage (Figure 10). Simulations without the inflow momentum term do not reproduce the initial roll on the opposite side of the damage. Without taking the inflow momentum into account the model rolls on the damage side. For lower initial stability $\overline{GM}_{0,1}$ the simulated roll response without inflow momentum flux has a transient angle on the damage side. In this case the flooding is continuous unlike in the experiments. Peculiarly the transient roll angle on the damage side is of the same magnitude than the first roll angle on the damage side in the measurements. For higher initial

stability $\overline{GM}_{0,2}$ in the simulation without the inflooding momentum flux the model heels to the damage side and attains the final equilibrium position without any transient roll.

When the inflow momentum flux is accounted for in the simulation the model rolls to the opposite side of the damage as in the measurements. For lower initial stability $\overline{GM}_{0,1}$ the first roll angle to the opposite side is slightly overestimated by the simulation. Due to this overestimation the damage opening is lifted above the water surface earlier and the flooding is stopped earlier than in the experiments. In the experiments the model rolls second time on the opposite side. In the simulation, at around 10 seconds, the roll motion is slowed down, like in the experiments, but the model rolls on the damage side. The roll motion at that time instant is slower when the biggest friction coefficient is used in the simulation.

At higher initial stability $\overline{GM}_{0,2}$ the magnitude of the first roll angle onto the opposite side corresponds to the measured one when the inflow momentum flux is accounted for. The period of the second roll angle is somewhat longer in the simulations than in the measurements. Due to this, the simulation is not at the same phase with the measurement but the roll decay and periods after the second roll angle correspond well to the measurement results. The floodwater amount corresponds well to the measurements when the inflow momentum flux is accounted for.

Asymmetric flooding on the damage side occurs in the transient flooding of the divided compartment Figure 11. The non-watertight longitudinal bulkheads in the compartment R21 slow down the cross-flooding and the model experiences a high roll angle on the damage side. After the first large roll, the

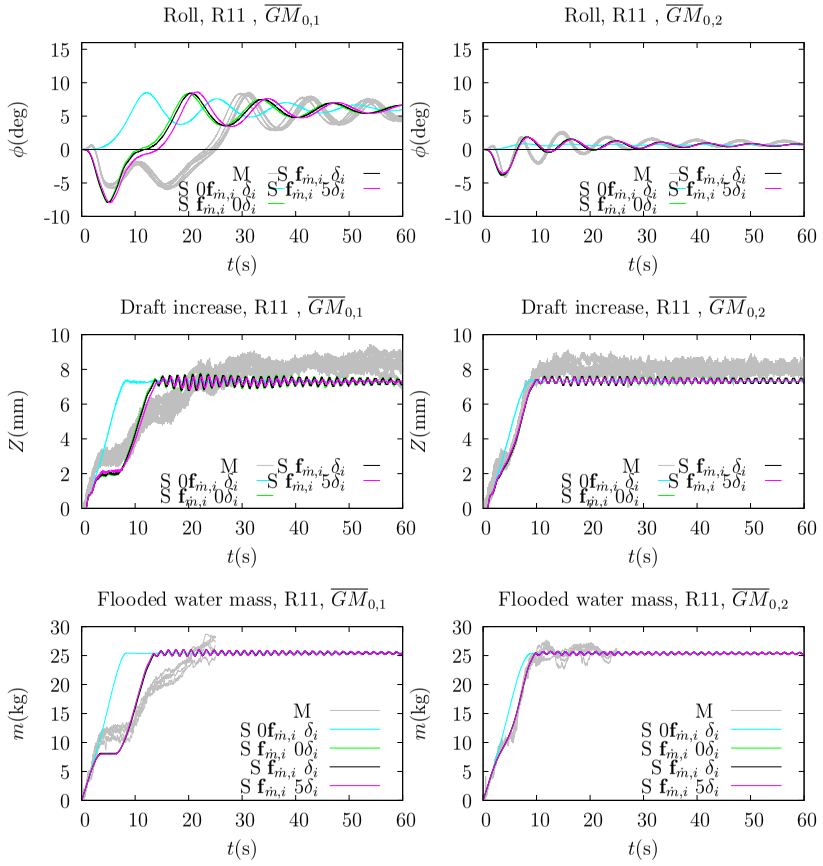

Figure 10: Transient flooding of undivided compartment R11.

model continues to roll on the damage side and decays to final equilibrium position on the same side. For smaller initial stability the initial roll angle and final equilibrium angle are bigger than for the higher initial stability. Otherwise the roll behaviour is similar at both initial stabilities. Simulation captures well the above described behaviour. The agreement between the simulated and measured roll angles is good. Accounting for the inflooding momentum flux has a minimal effect on the simulation results. The friction coefficient does not have any significant effect on the simulation of transient flooding of the divided compartment.

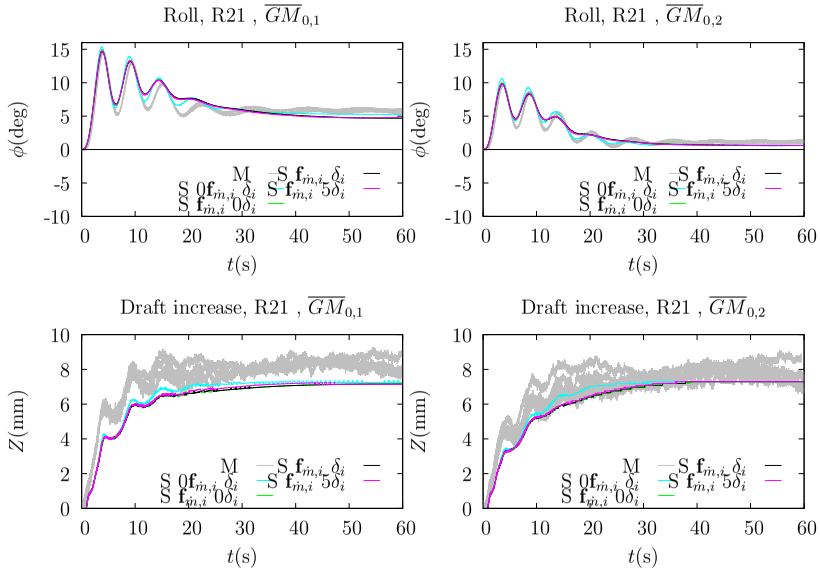

Figure 11: Transient flooding of divided compartment R21.

7. Discussion

7.1. Roll decay

Simulated roll decay in flooded condition is in good agreement with the experiments for the divided compartment cases. Roll angle magnitudes and periods as well as the roll time history match well the measured ones. The non-harmonic behaviour of the roll decay, with the undivided compartment R11 at low initial stability, was not totally captured by the simulation method. At lower fill amounts the friction coefficient seems to play an important role. The model for viscous dissipation at the walls does not seem to capture all the dissipation at the low fill heights. When the friction coefficient was increased the simulation agreed better with the measurements. The friction coefficient estimated by the dissipation of a standing wave does not take into account the wave breaking on the wall or high roll angles and room bottom which is not totally covered by the floodwater. The wave breaking can have an important contribution in the dissipation of the energy as pointed out by Bouscasse et al. (2014a,b). The damping of the floodwater motions at low fill heights requires a more elaborate model.

For the higher initial stability non-harmonic behaviour of roll was not observed in the measurements and the agreement with the simulations was also good. The roll period was estimated to be slightly longer in the simulations. The sloshing frequencies in the divided compartments are higher than the ship natural roll frequency. The higher frequency floodwater motion does not affect the ship roll. In a sense, the ship system filters out higher frequencies. For the undivided compartment the sloshing frequency is close to the ship natural roll frequency at low fill amount. In this case, the ship roll

motion is damped fast. At lower initial stability the total restoring moment is close to zero at a wide range of heel angle (see Figure 6). The roll motion takes part in a nearly labile area. The final equilibrium angle is nearly non-defined in a large range of angles. This results in a slow roll motions which are difficult to model. Small variations in the system can have big effect on the roll time history.

7.2. Transient flooding

Simulation model predicts the roll response well for flooding of the divided compartment. Inflow momentum does not have big effect in this case. Flooding of the undivided compartment is qualitatively well predicted. The inflow momentum has an important effect on the undivided compartment roll response. First roll angle onto the opposite side of the damage opening is reproduced in the simulation. Highest roll angle to the damage side is also predicted well. The magnitude of the roll, roll periods and damping are well reproduced. In case of the undivided compartment there is a deviation in the second roll angle. The simplifications in the modelling of some of the phenomena can lead to this small discrepancy.

Detailed surface profile is not modelled, which can be important at very shallow water cases as seen in the shallow water roll decay cases. Also the overestimation of the highest roll angle in the transient flooding case can be due to the viscous effects of the bore propagation at the beginning of the flooding and the water run-up at the opposite side (Bouscasse et al., 2014a,b). This could be overcome by applying a model through the friction factor, which could be updated to take these effects into account. Godderidge et al. (2012) have applied an impact model in their pendulum model. The

shortcoming of this approach is that it requires various parameter to be defined beforehand.

Furthermore, quasi-stationary flow through the opening was assumed. At the beginning of the flooding, following the abrupt introduction of the damage opening, the flow velocity through the opening is gained immediately. Entering fluid inertia is not included in the quasi-stationary hydraulic flow model. This could be overcome by applying a model that accounts for the inertia terms. However comparing the measured and simulated floodwater volumes this does not seem to be a major issue in the modelling.

Radiation forces on the ship hull were modelled with constant added mass and damping matrices, which were evaluated at the intact ship natural motion frequencies. This assumption neglects the fact that the damaged ship motions were non-harmonic in nature. The large roll angles and the increase in draft were not accounted for in the estimation of the added mass and damping. (Vassalos and Jasionowski, 2002) have shown that there can be significant difference in the hydrodynamic coefficients for damaged ship at high heel angles. However, based on this study, it remains difficult to estimate the consequences of applying constant hydrodynamic coefficients. This remains still an important topic for future studies.

In this study, the focus was on the transient roll response of the ship, concentrating on the inflooding jet, floodwater motions and the flow through the openings. The effects of the air compression and the wave action were not studied. Uncertainty in the air compression model is evaded by having the compartments fully ventilated. In reality the flooding process could be slower due to the trapped air in the compartment (Palazzi and de Kat, 2004;

Ruponen et al., 2013). The consequence of the slower flooding process to the roll can be in either direction depending on the case. To overcome this the in/outflow calculation in the presented simulation method could be extended with a method presented by Ruponen et al. (2007).

No wave action was applied in this study. In this way, the uncertainty on the wave modelling is evaded. In reality, the ship may be subject to wave action at the event of the abrupt flooding accident. However, this would require a study of huge numbers of cases, where the time instant of damage initiation would be varied with respect to the ship and wave position. The presented method is implemented with the possibility to take the wave action into account as in Matusiak (2013). The hull is presented with panels, thus enabling to account for the non-linear Froude-Krylov forces. The potential theory based calculation of the hydrodynamic coefficient also estimates the wave diffraction forces, which have not yet been implemented, but remains as a future work.

From the point of view of modelling the consequences of a collision or grounding accident of a ship, the model captures well the flooding phenomena and the transient roll response of the ship. Model tests results were reproduced well. The scale effect on these phenomena is still unknown when extending the simulation to ship accidents. In the simulation of consequences of an accident it is important to capture the direction of the first roll angle and the maximum angle. Differences in the direction of the roll and the magnitudes in angles can lead to totally different progression of the flooding inside the ship and to a totally different final stage.

8. Conclusions

The numerical non-linear time domain calculation method to simulate damage ship motions has been presented. In the method the key factors are modelled. The floodwater dynamics is based on the lumped mass method with a moving free surface. The ship and floodwater motions are fully coupled, mass variation in the flooded compartment and the inflooding momentum flux are accounted for. Simulated roll response and flooding process are compared to the model test data. The presented model does not require huge calculation resources. This allows for running a big number of simulations for the study of different factors on the flooding accident consequences. The simulation can also be performed in the real time. Following main conclusion can be drawn

- Simulated roll decay of the flooded ship agrees well with the model test results. For the cases with undivided compartment at lower initial stability there is a small difference in the varying roll period and for cases with undivided compartment at higher initial stability the simulated roll period is slightly longer. Viscous dissipation at smaller fill amounts need to be taken into account. For cases with divided compartment there is a good agreement between the simulated and the measured roll time histories.

- Simulation model predicts the roll response well for flooding of the divided compartment. Inflow momentum does not have big effect in this case

- Flooding of the undivided compartment is qualitatively well predicted.

The inflow momentum flux should be taken into account in this case. First roll angle onto the opposite side of the damage opening is reproduced in the simulation. Highest roll angle to the damage side is also predicted. The magnitude of the roll, roll periods and damping are well reproduced.

The applicability of the lumped mass method to model the coupled ship and floodwater motions has been systematically studied. In the study it is shown that the roll decay and transient flooding are extremely well predicted for the divided compartment. When the inflow momentum is accounted for the method is capable of predicting the transient flooding cases for the undivided compartment.

Acknowledgements

The research presented was carried out as a part of Fimecc's (Finnish Metals and Engineering Competence Cluster) research program Innovations and Network and was funded by Tekes (Finnish Funding Agency for Innovation).

References

Bouscasse, B., Colagrossi, A., Souto-Iglesias, A., Cercos-Pita, J. L., 2014a. Mechanical energy dissipation induced by sloshing and wave breaking in a fully coupled angular motion system. I. Theoretical formulation and numerical investigation. Physics of Fluids 26 (3).
URL http://scitation.aip.org/content/aip/journal/pof2/26/3/10.1063/1.4869233

Bouscasse, B., Colagrossi, A., Souto-Iglesias, A., Cercos-Pita, J. L., 2014b. Mechanical energy dissipation induced by sloshing and wave breaking in a fully coupled angular motion system. II. Experimental investigation. Physics of Fluids 26 (3).
URL http://scitation.aip.org/content/aip/journal/pof2/26/3/10.1063/1.4869234

Chang, B.-C., Blume, P., 1998. Survivability of damaged ro-ro passenger vessels. Schiffstechnik - Ship Technology Research 45, 105–117.

Dankowski, H., September 2012. An explicit progressive flooding simulation method. In: Proceedings of the 11th International Conference on the Stability of Ships and Ocean Vehicles. Athens, Greece.

de Kat, J. O., 2000. Dynamics of a ship with partially flooded compartment. In: Vassalos, D., Hamamoto, M., Papanikolaou, A., Molyneux, D. (Eds.), Contemporary Ideas on Ship Stability. Elsevier Science, pp. 249–263.

de Kat, J. O., van't Veer, R., September 2001. Mechanisms and physics leading to the capsize of damaged ships. In: Proceedings of the 5th International Ship Stability Workshop. Trieste, Italy.

Dillingham, J., 1981. Motion studies of a vessel with water on deck. Marine Technology 18 (1), 38–50.

Dodge, F. T., 1966. Analytical representation of lateral sloshing by equivalent mechanical models. In: Abrahamson, H. N. (Ed.), The dynamic behavior of liquids in moving containers, with applications to space vehicle technology. NASA.

Fossen, T. I., 2002. Marine control systems : guidance, navigation and control of ships, rigs and underwater vehicles. Marine Cybernetics, Trondheim.

Frank, W., October 1967. Oscillation of cylinders in or below the free surface of deep fluids. Tech. Rep. 2375, Naval Ship Research and Development Center, Washington, DC.

Fujiwara, T., Haraguchi, T., 2005. Roll motion of ro-ro passenger ship with flooded vehicle deck. International Journal of Offshore and Polar Engineering 15 (2), 109–116.

Gao, Z., Gao, Q., Vassalos, D., 2011. Numerical simulation of flooding of a damaged ship. Ocean Engineering 38.

Godderidge, B., Turnock, S. R., Tan, M., 2012. A rapid method for the simulation of sloshing using a mathematical model based on the pendulum equation. Computers & Fluids 57, 163–171.

Hashimoto, H., Kawamura, K., Sueyoshi, M., June 2013. Numerical method for damaged ships under flooding condition. In: Proceedings of the ASME 2013 32nd International Conference on Ocean, Offshore and Arctic Engineering. Nantes, France.

Ikeda, Y., Kamo, T., September 2001. Effects of transient motion in intermediate stages of flooding on the final condition of a damaged PCC. In: Proceedings of the 5th International Ship Stability Workshop. Trieste, Italy.

Ikeda, Y., Ma, Y., February 2000. An experimental study on large roll motion

in intermediate stage of flooding due to sudden ingress water. In: Proceedings of the 7th International Conference on Stability of Ships and Ocean Vehicles. Launceston, Tasmania, Australia, pp. 270–285.

Ikeda, Y., Shimoda, S., Takeuchi, Y., September 2003. Experimental studies on transient motion and time to sink of a damaged large passenger ship. In: Proceedings of the 8th International Conference on Stability of Ships and Ocean Vehicles. Madrid, Spain, pp. 243–252.

ITTC, September 2002. The Specialist Committee on Prediction of Extreme Ship Motions and Capsizing - Final Report and Recommendations to the 23rd ITTC. In: Proceedings of the 23rd ITTC. Vol. II. Venice, Italy, pp. 619–624.

ITTC, September 2005. The Specialist Committee on Stability in Waves - Final Report and Recommendations to the 24th ITTC. In: Proceedings of the 24th ITTC. Vol. II. Edinburgh, UK, pp. 369–408.

ITTC, September 2008. The Specialist Committee on Stabiliy in Waves - Final Report and Recommendations to the 25th ITTC. In: Proceedings of 25th ITTC. Vol. II. Fukuoka, Japan, pp. 611–624.

ITTC, August-September 2011. The Specialist Committee on Stabiliy in Waves - Final Report and Recommendations to the 26th ITTC. In: Proceedings of 26th ITTC. Vol. II. Rio de Janeiro, Brazil, pp. 523–560.

ITTC, August-September 2014. Stabiliy in Waves Committee - Final Report and Recommendations to the 27th ITTC. In: Proceedings of 27th ITTC. Vol. I. Copenhagen, Denmark, pp. 332–413.

Jasionowski, A., 2001. An integrated approach to damage ship survivability assessment. Ph.D. thesis, University of Strathclyde.

Journée, J. M. J., Vermeer, H., Vredeveldt, A. W., September 1997. Systematic model experiments on flooding of two ro-ro vessels. In: 6th International Conference on Stability of Ships and Ocean Vehicles. Varna, Bulgaria, pp. 81–98.

Keulegan, G. H., 1959. Energy dissipation in standing waves in rectangular basins. Journal of Fluid Mechanics 6, 35–50.

Khaddaj-Mallat, C., Rousset, J.-M., Ferrant, P., 2011. The transient and progressive flooding stages of damaged ro-ro vessels: A systematic review of entailed factors. Journal of Offshore Mechanics and Arctic Engineering 133 (3).

Manderbacka, T., Kulovesi, J., M. A. Celis C., Matusiak, J. E., Neves, M. A. S., 2014a. Model tests on the impact of the opening location on the water motions in a flooded tank with two compartments. Ocean Engineering 84, 67–80.
URL http://www.sciencedirect.com/science/article/pii/S0029801814001346

Manderbacka, T., Ruponen, P., Kulovesi, J., Matusiak, J. E., 20xx. Model experiments of the transient response to flooding of the box shaped barge. under review, submitted to Journal of Fluids and Structures on September 5, 2014.

Manderbacka, T. L., Jacob, V., Carriot, T., Mikkola, T., Matusiak, J. E., June 2014b. Sloshing forces on a tank with two compartments, application of the pendulum model and CFD. In: Proceedings of the ASME 2014 33nd International Conference on Ocean, Offshore and Arctic Engineering. San Francisco, California, USA.

Matusiak, J., 2013. Dynamics of a rigid ship. Aalto University, Helsinki, Finland.
URL https://aaltodoc.aalto.fi/handle/123456789/10265

Meyers, W. G., Sheridan, D. J., Salvesen, N., 1975. NSRDC ship-motion and sea-load computer program. Tech. Rep. 3376, NAVAL SHIP RESEARCH AND DEVELOPMENT CENTER BETHESDA MD.

Naito, S., Sueyoshi, M., September 2001. A numerical analysis of violent free surface flow on flooded car deck using particle method. In: Proceedings of the 5th International Ship Stability Workshop. Trieste, Italy.

Palazzi, L., de Kat, J., 2004. Model experiments and simulations of a damaged ship with air-flow taken into account. Marine Technology 41 (1), 38 – 44.

Papanikolaou, A., Zaraphonitis, G., Spanos, D., Boulougouris, E., Elipoulou, E., February 2000. Investigation into the capsizing of damaged ro-ro passenger ships in waves. In: Proceedings of the 7th International Conference on Stability of Ships and Ocean Vehicles. Launceston, Tasmania, Australia, pp. 351–362.

Perez, T., 2005. Ship motion control : course keeping and roll stabilisation using rudder and fins. Springer.

Ruponen, P., 2007. Progressive flooding of a damaged passenger ship. Ph.D. thesis, Helsinki University of Technology, Ship Laboratory.
URL http://lib.tkk.fi/Diss/2007/isbn9789512290130/isbn9789512290130.pdf

Ruponen, P., Kurvinen, P., Saisto, I., Harras, J., 2013. Air compression in a flooded tank of a damaged ship. Ocean Engineering 57 (0), 64 – 71.
URL http://www.sciencedirect.com/science/article/pii/S002980181200368X

Ruponen, P., Sundell, T., Larmela, M., 2007. Validation of a simulation method for progressive flooding. International Shipbuilding Progress 54 (4), 305–321.
URL http://iospress.metapress.com/content/M771026653VH163G

Sadat-Hosseini, H., Kim, D. H., Lee, S. K., Rhee, S. H., Carrica, P., Stern, F., Rhee, K.-P., September 2012. CFD and EFD Study of Damaged Ship Stability in Calm Water and Regular Waves. In: Proceedings of the 11th International Conference on the Stability of Ships and Ocean Vehicles. Athens, Greece.

Salvesen, N., Tuck, E. O., Faltinsen, O., 1970. Ship motions and sea loads. SNAME Transactions 78, 250–287.

Santos, T. A., Guedes Soares, C., 2008. Study of damaged ship motions taking into account floodwater dynamics. Journal of Marine Science and Technology 13 (3), 291–307.

Santos, T. A., Guedes Soares, C., 2009. Numerical assessment of factors affecting the survivability of damaged roro ships in waves. Ocean Engineering 36 (11), 797 – 809.
URL http://www.sciencedirect.com/science/article/pii/S0029801809000961

Santos, T. A., Winkle, I. E., Guedes Soares, C., 2002. Time domain modelling of the transient asymmetric flooding of ro-ro ships. Ocean Engineering 29 (6), 667–688.

Schreuder, M., Hogström, P., Ringsberg, J., Johnson, E., Janson, C.-E., 2011. A method for assessment of the survival time of a ship damaged by collision. Journal of Ship Research 55 (2), 86–99.

Shen, L., Vassalos, D., June 2009. Applications of 3d parallel SPH for sloshing and flooding. In: Proceedings of the 10th International Conference on Stability of Ships and Ocean Vehicles. St. Petersburg, Russia.

Silverman, S., Abrahamson, H. N., 1966. Damping of liquid motions and lateral sloshing. In: Abrahamson, H. N. (Ed.), The dynamic behavior of liquids in moving containers, with applications to space vehicle technology. NASA.

Souto-Iglesias, A., Macia, F., González, L. M., Cercos-Pita, J. L., 2013. On the consistency of MPS. Computer Physics Communications 184 (3), 732 – 745.

URL http://www.sciencedirect.com/science/article/pii/S0010465512003852

Souto-Iglesias, A., Macia, F., González, L. M., Cercos-Pita, J. L., 2014. Addendum to on the consistency of mps [comput. phys. comm. 184 (3) (2013) 732745]. Computer Physics Communications 185 (2), 595 – 598.
URL http://www.sciencedirect.com/science/article/pii/S0010465513003469

Spanos, D., Papanikolaou, A., 2001. On the stability of fishing vessels with trapped water on deck. Ship Technology Research-Schiffstechnik 48, 124–133.

Spouge, J. R., 1985. The Technical Investigation of the Sinking of the Ro-Ro Ferry European Gateway. Transactions of RINA 127, 49–72.

Touzé, D. L., Marsh, A., Oger, G., Guilcher, P.-M., Khaddaj-Mallat, C., Alessandrini, B., Ferrant, P., 2010. SPH simulation of green water and ship flooding scenarios. Journal of Hydrodynamics, Ser. B 22 (5, Supplement 1), 231 – 236.
URL http://www.sciencedirect.com/science/article/pii/S1001605809601992

Valanto, P., 2008. Research study on the sinking sequence and evacuation of the MV Estonia - final report. Tech. Rep. 1663, HSVA, Hamburg, Germany.
URL http://www.hsva.de/10_downloads_content/HSVA1663FINAL.pdf

van Walree, F., Papanikolaou, A., August 2007. Benchmark study of numerical codes for the prediction of time to flood of ships: Phase i. In: Proceedings of the 9th International Ship Stability Workshop. Hamburg, Germany.

van't Veer, R., de Kat, J. O., February 2000. Experimental and numerical investigation on progressive flooding and in complex compartment geometries. In: Proceedings of the 7th International Conference on Stability of Ships and Ocean Vehicles. Launceston, Tasmania, Australia, pp. 305–321.

Vassalos, D., Jasionowski, A., October 2002. Damaged ship hydrodynamics. In: Proceedings of the 6th International Ship Stability Workshop. Glen Cove, NY, USA.

Vredeveldt, A. W., Journée, J. M. J., April 1991. Roll motions of ships due to sudden water ingress, calculations and experiments. In: RINA'91, International Conference on Ro-Ro Safety and Vulnerability the Way Ahead. London, England.

Ypma, E. L., Turner, T., June 2010. An approach to the validation of ship flooding simulation models. In: Proceedings of the 11th International Ship Stability Workshop. Wageningen, Netherlands.

Zaraphonitis, G., Papanikolaou, A., Spanos, D., September 1997. On a 3-D mathematical model of the damage stability of ships in waves. In: 6th International Conference on Stability of Ships and Ocean Vehicles. Vol. 1. Varna, Bulgaria, pp. 81–98.